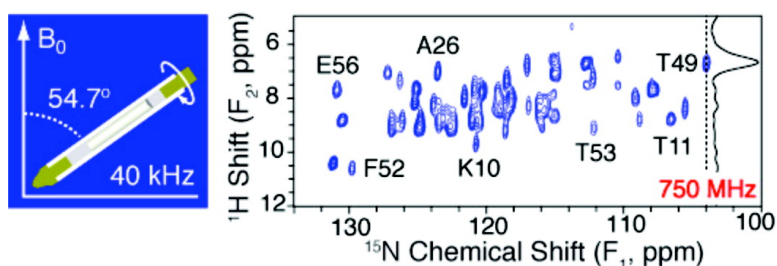## Article

Proton-Detected Solid-State NMR Spectroscopy of Fully Protonated Proteins at 40 kHz Magic-Angle Spinning

Donghua H. Zhou, Gautam Shah, Mircea Cormos, Charles Mullen, Dennis Sandoz, and Chad M. Rienstra

More About This Article

Additional resources and features associated with this article are available within the HTML version:

- Supporting Information
- Links to the 14 articles that cite this article, as of the time of this article download
- Access to high resolution figures
- Links to articles and content related to this article
- Copyright permission to reproduce figures and/or text from this article

View the Full Text HTML

Proton-Detected Solid-State NMR Spectroscopy of Fully Protonated Proteins at 40 kHz Magic-Angle Spinning

Donghua H. Zhou,[†] Gautam Shah,[†] Mircea Cormos,[‖] Charles Mullen,[‖]
Dennis Sandoz,[⊥] and Chad M. Rienstra*,[†,‡,§]

Contribution from the Departments of Chemistry and Biochemistry and Center for Biophysics and Computational Biology, University of Illinois at Urbana-Champaign, Urbana, Illinois 61801, Varian, Inc., 2607 Midpoint Drive, Fort Collins, Colorado 80525, and Varian, Inc., 3120 Hansen Way, Palo Alto, California 94304

Received May 15, 2007; E-mail: rienstra@scs.uiuc.edu

Abstract: Remarkable progress in solid-state NMR has enabled complete structure determination of uniformly labeled proteins in the size range of 5−10 kDa. Expanding these applications to larger or mass-limited systems requires further improvements in spectral sensitivity, for which inverse detection of ^{13}C and ^{15}N signals with ^{1}H is one promising approach. Proton detection has previously been demonstrated to offer sensitivity benefits in the limit of sparse protonation or with ~30 kHz magic-angle spinning (MAS). Here we focus on experimental schemes for proteins with ~100% protonation. Full protonation simplifies sample preparation and permits more complete chemical shift information to be obtained from a single sample. We demonstrate experimental schemes using the fully protonated, uniformly $^{13}C,^{15}N$-labeled protein GB1 at 40 kHz MAS rate with 1.6-mm rotors. At 500 MHz proton frequency, 1-ppm proton line widths were observed (500 ± 150 Hz), and the sensitivity was enhanced by 3 and 4 times, respectively, versus direct ^{13}C and ^{15}N detection. The enhanced sensitivity enabled a family of 3D experiments for spectral assignment to be performed in a time-efficient manner with less than a micromole of protein. CANH, CONH, and NCAH 3D spectra provided sufficient resolution and sensitivity to make full backbone and partial side-chain proton assignments. At 750 MHz proton frequency and 40 kHz MAS rate, proton line widths improve further in an absolute sense (360 ± 115 Hz). Sensitivity and resolution increase in a better than linear manner with increasing magnetic field, resulting in 14 times greater sensitivity for ^{1}H detection relative to that of ^{15}N detection.

Introduction

Dramatic progress has been achieved to enable complete protein structures to be determined by solid-state NMR (SS-NMR) methods.[1,2] Many of the advances have been intended for uniformly $^{13}C,^{15}N$-enriched proteins using multidimensional methods, which investigators have rapidly applied to proteins such as BPTI,[3] SH3,[4] and ubiquitin,[5] as well as more challenging biomolecular systems. For example, studies of membrane proteins have provided insights into the residues involved in toxin-induced conformational changes of a potassium channel[6]

and the organization and dynamics of a seven-transmembrane helix receptor.[7] Similarly, rapid progress has enabled studies of fibrous proteins, such as β-amyloid,[8−10] α-synuclein,[11] and HET-s prion.[12] In many of these studies, multidimensional methods permitted efficient analysis of large protein domains. Nevertheless, sensitivity remains a significant limitation in many contexts, and expanding the range of biological SSNMR applications requires improvements in this area. Beyond reducing required measurement times and tackling larger and more biologically complex systems, improved sensitivity promises to open new areas of study; for example, mammalian membrane proteins are notoriously difficult to express in milligram quantity, especially with isotopic (^{13}C, ^{15}N) labels. Better NMR methods are required for these reasons.

† Department of Chemistry, University of Illinois at Urbana-Champaign.
‡ Department of Biochemistry, University of Illinois at Urbana-Champaign.
§ Center for Biophysics and Computational Biology, University of Illinois at Urbana-Champaign.
‖ Varian, Inc., Fort Collins, CO.
⊥ Varian, Inc., Palo Alto, CA.

 (1) Castellani, F.; van Rossum, B.; Diehl, A.; Schubert, M.; Rehbein, K.; Oschkinat, H. *Nature* **2002**, *420*, 98−102.
 (2) Lange, A.; Becker, S.; Seidel, K.; Giller, K.; Pongs, O.; Baldus, M. *Angew. Chem., Int. Ed.* **2005**, *44*, 2089−2092.
 (3) McDermott, A.; Polenova, T.; Bockmann, A.; Zilm, K. W.; Paulsen, E. K.; Martin, R. W.; Montelione, G. T. *J. Biomol. NMR* **2000**, *16*, 209−219.
 (4) Pauli, J.; Baldus, M.; van Rossum, B.; de Groot, H.; Oschkinat, H. *ChemBioChem* **2001**, *2*, 101−110.
 (5) Igumenova, T. I.; Wand, A. J.; McDermott, A. E. *J. Am. Chem. Soc.* **2004**, *126*, 5323−5331.

 (6) Lange, A.; Giller, K.; Hornig, S.; Martin-Eauclaire, M.-F.; Pongs, O.; Becker, S.; Baldus, M. *Nature* **2006**, *440*, 959−962.
 (7) Etzkorn, M.; Martell, S.; Andronesi, O. C.; Seidel, K.; Engelhard, M.; Baldus, M. *Angew. Chem., Int. Ed.* **2007**, *46*, 459−462.
 (8) Petkova, A. T.; Buntkowsky, G.; Dyda, F.; Leapman, R. D.; Yau, W. M.; Tycko, R. *J. Mol. Biol.* **2004**, *335*, 247−260.
 (9) Petkova, A. T.; Leapman, R. D.; Guo, Z. H.; Yau, W. M.; Mattson, M. P.; Tycko, R. *Science* **2005**, *307*, 262−265.
(10) Tycko, R. *Curr. Opin. Struct. Biol.* **2000**, *4*, 500−506.
(11) Heise, H.; Hoyer, W.; Becker, S.; Andronesi, O. C.; Riedel, D.; Baldus, M. *Proc. Natl. Acad. Sci. U.S.A.* **2005**, *102*, 15871−15876.
(12) Ritter, C.; Maddelein, M. L.; Siemer, A. B.; Luhrs, T.; Ernst, M.; Meier, B. H.; Saupe, S. J.; Riek, R. *Nature* **2005**, *435*, 844−848.

Here we focus on detection of ^{1}H signals, a sensitivity enhancement technique widely used in solution NMR[13] but not yet routinely applied in the solid state because of strong dipolar couplings among ^{1}H spins, which under standard magic-angle spinning (MAS) conditions (rates of ~5−15 kHz) result in ^{1}H line widths of several kilohertz. One promising approach is to employ MAS rates of ~40 kHz or greater by using small MAS rotors (diameter less than 2.0 mm). Although sample volumes are less than 10 μL, the better filling factor results in absolute sensitivity rivaling much larger quantities of protein in larger diameter coils. Previous investigators demonstrated convincing benefits of proton detection for peptides and proteins in the 10−30 kHz regime with spin dilution,[14] and even with natural abundance compounds with ~30 kHz spinning.[15,16] Very high resolution spectra (rivaling solution NMR) have been demonstrated by combining isotopic dilution and ~10−20 kHz MAS rates.[17−19] Investigators continue to push the limits of MAS rates, and recent reports of ^{13}C-detected protein spectra at >60 kHz MAS rates have led to substantial benefits in terms of resolution and sensitivity (Pintacuda, G.; Steuernagel, S.; Engelke, F.; Pieratelli, R.; Bertini, I.; Emsley, L. Laboratoire de Chimie, Ecole Normale Supérieure de Lyon, Private communication, 2007).

These recent advances not only represent substantial technical progress for biomolecular solid-state NMR, but also more importantly expand opportunities for a variety of new chemical applications including the study of protein−solvent interactions in microcrystals,[20−23] the examination of mass-limited samples at natural abundance, robust studies of nuclei near paramagnetic centers,[24] and measurements of proton−proton correlations that report upon long-range internuclear distances.[23,25] Detailed understanding of ^{1}H chemical shifts and their relationship to chemical bonding and structure will aid in high-resolution structure determination, as well as the analysis of pharmaceutical formulations.[26]

In this study, we address the challenges of studying fully protonated proteins. Although deuteration protocols are readily applicable to many soluble proteins,[27] they remain impractical for many membrane proteins,[28] in which back-exchange of the amide deuterons to protons also may be very slow and/or strongly dependent upon position in the protein sequence.[29] Although this fundamentally interesting phenomenon yields insight into protein dynamics,[30,31] it presents a severe problem for detecting all sites in a protein. Likewise in protein fibrils, site-specific rates of exchange may be of interest to measure experimentally;[32] to do so starting with a lack of protons may present a problem for measuring the slow rates (i.e., a deuterated sample prepared as fibrils and then exposed to H_2O). Also in industrial applications, such as with therapeutic proteins, it is necessary to examine samples analytically in preparations identical to the formulations used in the clinic; isotopic labeling may not be permissible.[33] Therefore, it is desirable to acquire high-resolution protein spectra without the need for any type of isotopic labeling. Full protonation also results in a situation where more complete chemical shift information can be obtained with a single sample, such as side-chain chemical shifts. Finally, full protonation leads to interesting spin dynamics.

With this rationale, we investigate fast MAS SSNMR spectroscopy of fully protonated peptides and proteins. First, we examine a model peptide, *N*-acetylvaline (NAV), for comparison with earlier work at 5−25 kHz MAS rates[34] and for evaluation of instrument performance at 500 MHz. Second, we apply these results to a solvated, microcrystalline protein, the B1 immunoglobulin binding domain of protein G (GB1). Effective solvent suppression, with a mother liquor composed of protonated solvents (H_2O, methylpentanediol, and 2-propanol), requires modifications to previous techniques, which we describe in detail. Third, 2D spectra involving indirect and direct ^{1}H dimensions enable a comparison of the [1]H- and X-detected spectra for both ^{15}N and ^{13}C in GB1, to evaluate sensitivity as well as resolution in relatively simple experiments. Fourth, we implement 3D pulse sequences involving proton detection to assign the HN and HA sites in GB1. This is the first report of the proton shifts of GB1 in its microcrystalline preparation. Finally, we demonstrate the sensitivity and resolution benefits of using higher magnetic fields (750 MHz versus 500 MHz) in combination with 40 kHz MAS, which are better than linear in magnetic field.

Experimental Section

Sample Preparation. Uniformly ^{13}C,[15]N-labeled NAV was synthesized via solution methods and recrystallized by slow evaporation from methanol solution. A nanocrystalline sample of uniformly ^{13}C,[15]N-labeled protein GB1 (T2Q mutant) was prepared according to Franks et al.;[35] natural abundance methyl-2,4-pentanediol (MPD) and 2-propanol (IPA) from Sigma-Aldrich were used as precipitants in a 2:1 volume ratio of MPD/IPA, adding 3.5 equiv of this solution to the protein solution, which was at a concentration of ~30 mg/mL. When packing the protein sample into the 1.6-mm MAS rotor, rubber discs were inserted above and below the sample to maintain an airtight seal. The total quantity of material packed into the rotor was 9 mg, of which slightly more than half by mass (~5 mg, ~0.9 μmol) was estimated to be GB1, based on experience with packing many such GB1 samples

(13) Bodenhausen, G.; Ruben, D. J. *Chem. Phys. Lett.* **1980**, *69*, 185−189.
(14) McDermott, A. E.; Creuzet, F. J.; Kolbert, A. C.; Griffin, R. G. *J. Magn. Reson.* **1992**, *98*, 408−413.
(15) Ishii, Y.; Tycko, R. *J. Magn. Reson.* **2000**, *142*, 199−204.
(16) Ishii, Y.; Yesinowski, J. P.; Tycko, R. *J. Am. Chem. Soc.* **2001**, *123*, 2921−2922.
(17) Agarwal, V.; Diehl, A.; Skrynnikov, N.; Reif, B. *J. Am. Chem. Soc.* **2006**, *128*, 12620−12621.
(18) Chevelkov, V.; Rehbein, K.; Diehl, A.; Reif, B. *Angew. Chem., Int. Ed.* **2006**, *45*, 3878−3881.
(19) Paulson, E. K.; Morcombe, C. R.; Gaponenko, V.; Dancheck, B.; Byrd, R. A.; Zilm, K. W. *J. Am. Chem. Soc.* **2003**, *125*, 15831−15836.
(20) Bockmann, A.; Juy, M.; Bettler, E.; Emsley, L.; Galinier, A.; Penin, F.; Lesage, A. *J. Biomol. NMR* **2005**, *32*, 195−207.
(21) Lesage, A.; Bockmann, A. *J. Am. Chem. Soc.* **2003**, *125*, 13336−13337.
(22) Lesage, A.; Emsley, L.; Penin, F.; Bockmann, A. *J. Am. Chem. Soc.* **2006**, *128*, 8246−8255.
(23) Paulson, E. K.; Morcombe, C. R.; Gaponenko, V.; Dancheck, B.; Byrd, R. A.; Zilm, K. W. *J. Am. Chem. Soc.* **2003**, *125*, 14222−14223.
(24) Pintacuda, G.; Giraud, N.; Pierattelli, R.; Bockmann, A.; Bertini, I.; Emsley, L. *Angew. Chem., Int. Ed.* **2007**, *46*, 1079−1082.
(25) Lange, A.; Seidel, K.; Verdier, L.; Luca, S.; Baldus, M. *J. Am. Chem. Soc.* **2003**, *125*, 12640−12648.
(26) Zell, M. T.; Padden, B. E.; Grant, D. J. W.; Chapeau, M. C.; Prakash, I.; Munson, E. J. *J. Am. Chem. Soc.* **1999**, *121*, 1372−1378.
(27) Gardner, K. H.; Kay, L. E. *Annu. Rev. Biophys. Biomol. Struct.* **1998**, *27*, 357−406.
(28) Bonander, N.; Hedfalk, K.; Larsson, C.; Mostad, P.; Chang, C.; Gustafsson, L.; Bill, R. M. *Protein. Sci.* **2005**, *14*, 1729−1740.

(29) Baenziger, J. E.; Methot, N. *J. Biol. Chem.* **1995**, *270*, 29129−29137.
(30) Cotten, M.; Fu, R.; Cross, T. A. *Biophys. J.* **1999**, *76*, 1179−1189.
(31) Huo, S.; Arumugam, S.; Cross, T. A. *Solid State Nucl. Magn. Reson.* **1996**, *7*, 177−183.
(32) Lu, X.; Wintrode, P. L.; Surewicz, W. K. *Proc. Natl. Acad. Sci. U.S.A.* **2007**, *104*, 1510−1515.
(33) Carter, P. J. *Nat. Rev. Immunol.* **2006**, *6*, 343−357.
(34) Zhou, D. H.; Graesser, D. T.; Franks, W. T.; Rienstra, C. M. *J. Magn. Reson.* **2006**, *178*, 297−307.
(35) Franks, W. T.; Zhou, D. H.; Wylie, B. J.; Money, B. G.; Graesser, D. T.; Frericks, H. L.; Sahota, G.; Rienstra, C. M. *J. Am. Chem. Soc.* **2005**, *127*, 12291−12305.
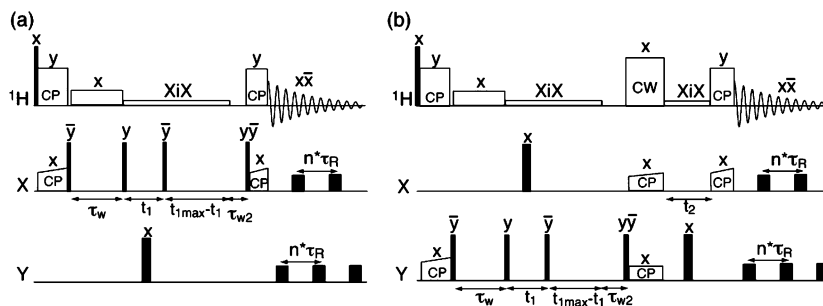
Figure 1. Proton-detected pulse sequences used in this study. (a) Sequence for NH 2D (X = ^{15}N, Y = ^{13}C) and CH 2D (X = ^{13}C, Y = ^{15}N) experiments. (b) 3D sequence for CANH and CONH (X = ^{15}N, Y = ^{13}C), as well as NCAH (X = ^{13}C, Y = ^{15}N). Narrow and wide rectangles represent $\pi/2$ and π pulses, respectively; weaker π pulses were used during acquisition. TPPI[64] (at 500 MHz) or States-TPPI[65,66] (at 750 MHz) was applied to the $\pi/2$ or spin lock pulse immediately following the indirect evolution periods to ensure that residual artifacts were segregated to the edges of the indirect dimensions. Two-step phase cycles as indicated in the figure were adequate to ensure proper coherence selection and solvent suppression. Additional calibrations of transmitter or receiver phases specifically for these experiments were not necessary.

in our laboratory in larger rotors, as well as comparisons of the total integrated intensity of the ^{13}C spectra relative to the model compounds used to configure the instrument.

NMR Experiments. Most of the SSNMR experiments in this study were performed on a 500 MHz Varian (Palo Alto, CA and Fort Collins, CO) Infinity Plus spectrometer. The Varian FastMAS ^{1}H$-^{13}$C$-^{15}$N probes were equipped with 1.6-mm spinning modules. For the 500 MHz probe, used in triple resonance mode, ^{1}H, ^{13}C, and ^{15}N $\pi/2$ pulse widths were 1.05, 1.44, and 2.44 μs with 148, 418, and 221 W input power levels, respectively. The relative channel efficiencies for this probe were $(B_{1W})^H/(B_{1W})^X = 0.58$ for X = ^{13}C and 0.28 for X = ^{15}N, where B_{1W} was the B_1 field generated by unit input power.[19] Experiments were performed at 40 kHz MAS rate (± 15 Hz) except for a subset of the proton 1D spectra in the model compound NAV. The cooling gas was regulated at 0 °C, and the actual sample temperature was 25 $\pm$ 5 °C because of frictional heating induced by 40 kHz MAS. Chemical shifts were referenced to DSS using adamantane as a secondary standard.[36]

For comparison at higher magnetic field, additional experiments were performed on a 750 MHz Varian INOVA spectrometer with a BioFastMAS ^{1}H$-^{13}$C$-^{15}$N probe (Varian) equipped with a 1.6-mm spinning module and a scroll coil for reduced radio frequency (rf) heating.[37] ^{1}H, ^{13}C, and ^{15}N $\pi/2$ pulse widths were 1.75, 3.8, and 4.0 μs with 208, 356, and 984 W input power levels, respectively. The relative channel efficiencies for this probe were $(B_{1W})^H/(B_{1W})^X = 0.71$ for X = ^{13}C and 0.50 for X = ^{15}N.

Solution backbone assignments of GB1 were made according to Gronenborn et al.[38] with minor changes near the T2Q mutation site.[35] To confirm HA and side-chain proton assignments, HCCH-TOCSY and NOESY-HSQC experiments were performed on a 600 MHz Varian UnityINOVA triple resonance spectrometer, using the BioPack interface in VNMR version 6.1D (Varian, Palo Alto, CA).

Pulse Sequences. For the dry NAV sample, the 2D HETCOR experiments did not require solvent suppression and thus previously published pulse sequences were satisfactory.[34] For the GB1 sample, modifications to proton-detected sequences (Figure 1) were required to suppress multiple solvent resonances of water and the alcohol precipitants. A pulse of moderate power (~ 40 kHz or less) was applied for a sufficiently long duration ($\tau_w = 300$ ms) to saturate solvent signals; we used such saturation periods before evolution periods to avoid polarization transfers due to homonuclear recoupling among X or Y nuclei (although the homonuclear recoupling effects were extremely small at such a high MAS rate). A short T_2 filter ($\tau_{w2} = 10$ ms) was also added to further attenuate any residual solvent signals. The precise

^{1}H carrier position was not critical but conveniently placed on one of the solvent resonances. We refer to the ^{1}H-to-X (where X = ^{15}N or ^{13}C) cross-polarization (CP) step as "HX" and the X-to-^{1}H as "XH"; likewise, the correlation experiments are referred to as "HX" and "XH" for the X- and ^{1}H-detected experiments, respectively. During HX and XH CP, a tangent ramp was applied to the ^{1}H channel with shape parameters ($\Delta = 9$ kHz and $b_f = 5$ kHz according to notations used in ref 39) optimized for the best sensitivity.[39] The mean rf fields were 100 and 60 kHz for ^{1}H and X channels, respectively; these nutation frequencies correspond to half-integer multiples of the spinning rate ($\omega_H = {}^5/_2\omega_R$ and $\omega_C = {}^3/_2\omega_R$) to avoid rotary resonance recoupling[40] during the CP period. The YX transfer was achieved with SPECIFIC CP,[41] using a double-quantum condition with rf nutation frequencies of ~ 10, ~ 30, and 150 kHz for ^{13}C, ^{15}N, and ^{1}H channels, respectively. Low-power XiX decoupling[42] of ~ 12 kHz was applied during indirect evolution periods. ^{13}C and ^{15}N π pulses during indirect evolution periods were at the maximal field amplitude (according to the $\pi/2$ pulses quoted earlier) and reduced to half the field strength for decoupling during the acquisition period. These π pulses were applied once every 40 rotor periods, with rotor synchronization and *XY*-16 supercycling.[43]

Processing and Analysis. Spectra were processed using NMRPipe,[44] with detailed processing parameters provided in the figure captions. Chemical shift assignments for ^{15}N and ^{13}C in GB1 as previously reported[35] were utilized to identify correlations to ^{1}H signals. Peak picking was performed in Sparky version 3.112 (Goddard, T. D.; Kneller, D. G. University of California: San Francisco, CA, 2006). Line-shape fitting was performed with DMFIT.[45]

Results and Discussion

A. Model Compound Studies. One-dimensional ^{1}H spectra as a function of MAS rate for NAV (Figure 2) illustrate substantial improvements in resolution at 40 kHz. Previous investigators have identified a linear relationship between inverse spinning rate and proton line width[46] when the homogeneous rate of decay dictates resolution (i.e., in the limit of small

(36) Morcombe, C. R.; Zilm, K. W. *J. Magn. Reson.* **2003**, *162*, 479−486.
(37) Stringer, J. A.; Bronnimann, C. E.; Mullen, C. G.; Zhou, D. H.; Stellfox, S. A.; Li, Y.; Williams, E. H.; Rienstra, C. M. *J. Magn. Reson.* **2005**, *173*, 40−48.
(38) Gronenborn, A. M.; Filpula, D. R.; Essig, N. Z.; Achari, A.; Whitlow, M.; Wingfield, P. T.; Clore, G. M. *Science* **1991**, *253*, 657−661.

(39) Hediger, S.; Meier, B. H.; Ernst, R. R. *Chem. Phys. Lett.* **1995**, *240*, 449−456.
(40) Oas, T. G.; Griffin, R. G.; Levitt, M. H. *J. Chem. Phys.* **1988**, *89*, 692−695.
(41) Baldus, M.; Petkova, A. T.; Herzfeld, J. H.; Griffin, R. G. *Mol. Phys.* **1998**, *95*, 1197−1207.
(42) Ernst, M.; Samoson, A.; Meier, B. H. *J. Magn. Reson.* **2003**, *163*, 332−339.
(43) Gullion, T.; Baker, D. B.; Conradi, M. S. *J. Magn. Reson.* **1990**, *89*, 479−484.
(44) Delaglio, F.; Grzesiek, S.; Vuister, G. W.; Zhu, G.; Pfeifer, J.; Bax, A. *J. Biomol. NMR* **1995**, *6*, 277−293.
(45) Massiot, D.; Fayon, F.; Capron, M.; King, I.; Calvé, S. L.; Alonso, B.; Durand, J.-O.; Bujoli, B.; Gan, Z.; Hoatson, G. *Magn. Reson. Chem.* **2002**, *40*, 70−76.
(46) Filip, C.; Hafner, S.; Schnell, I.; Demco, D. E.; Spiess, H. W. *J. Chem. Phys.* **1999**, *110*, 423−440.
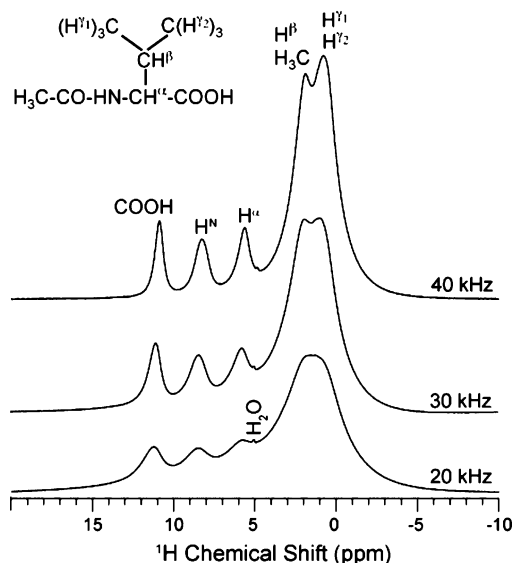
Figure 2. Bloch decay ¹H MAS spectra of NAV as a function of spinning rate (500 MHz ¹H frequency).

inhomogeneous broadening). Here we analyze the line widths by fitting each spectrum with five Lorentzian lines (neglecting the small residual water peak) using software DMFIT.[45] The amide HN line width was 858, 556, and 442 Hz at 20, 30, and 40 kHz MAS, respectively; the HA line width likewise was 1332, 693, and 426 Hz. At 40 kHz, the HN line width was slightly more than half of the observed value at 20 kHz, consistent with the linear dependence noted earlier. The HA line width decreased more rapidly with inverse spinning rate, likely because of the presence of multiple strong coupling partners (i.e., the HN and HB). Since the enhancement factor for indirect detection is proportional to the square root of the proton line width,[16,19] this 3-fold reduction in line width upon increasing the spinning rate from 20 to 40 kHz is expected to have approximately a 73% benefit for sensitivity at higher MAS rates.

HETCOR 2D experiments were performed at 40 kHz MAS rate to assess signal enhancement relative to low gyromagnetic ratio detection. To obtain reliable enhancement factors (ξ) from directly and indirectly detected HETCOR 2D experiments, we set the maximum t_1 and t_2 evolution times to $\sim kT_2$, where T_2 is the spin–spin relaxation time as measured in a Hahn echo[47] experiment for each nucleus, and k is a value typically between 1 and 3. In this study, we chose $k = 3$ to give the most accurate report of the inherent resolution; smaller values for k favor sensitivity and are likely to be preferred in sensitivity-limited applications.[19] The NAV T_2 values under these conditions are 1.4 ± 0.1 ms for HN, 1.2 ± 0.1 ms for HA, 36 ± 1 ms for amide ¹⁵N, and effectively 3.6 ms for CA because homonuclear decoupling was not employed here. The "intrinsic" T_2 for CA was 8.4 ms, which was extracted after deconvolution of both CA–C′ and CA–CB J-couplings. The value of 3.6 ms takes the cosine modulation into account to good approximation. Each dimension was zero filled, but no apodization function was applied.

The HA–CA peak has a signal-to-noise ratio (SNR) of 205 in the ¹³C-detected HC 2D spectrum (Figure 3a) and SNR = 887 in the ¹H-detected CH 2D (Figure 3b). Compensating for
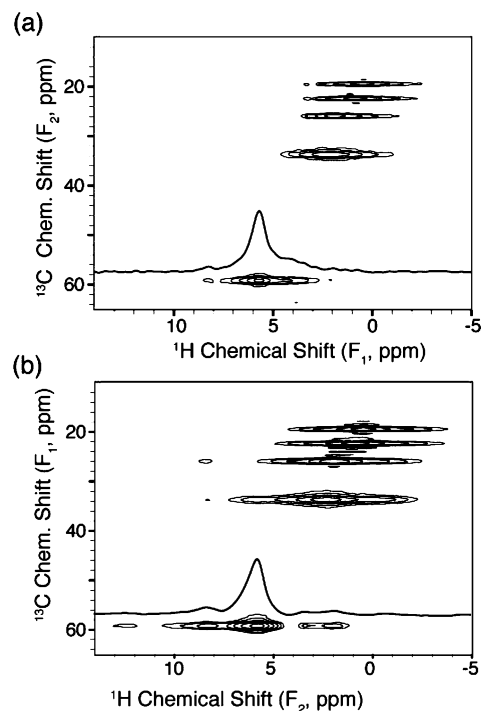
(47) Hahn, E. L. *Phys. Rev.* **1950**, *80*, 580–594.

Figure 3. Heteronuclear ¹³C–¹H 2D correlation spectra of fully protonated NAV (500 MHz ¹H frequency). Pulse sequences were used as reported previously,[34] with 40 kHz MAS, 2.2-s recycle delay, and 12.5-μs dwell time. The indirect dimension was sampled with TPPI.[64] No apodization was applied in the processing. (a) ¹³C-detected HC 2D spectrum acquired with 312 t_1 increments, eight scans per increment, and 0.05-ms HC CP contact time. The lowest contour is drawn at 10 times the rms noise floor (10σ) and spaced by a factor of 2.0. (b) ¹H-detected CH 2D spectrum acquired with 890 t_1 increments, and four scans per increment. The contact times were 2 ms for the initial HC CP and 0.05 ms for the final CH CP. Contours start at 20σ and are spaced by a factor of 2.0.

the difference in total number of scans (the product of number of t_1 increments and scans per increment), the enhancement is calculated as $\xi = (887/205)(312*8/890*4)^{1/2} = 3.6$. To minimize spectral overlap, a short contact time (0.05 ms) was used for the CP period that establishes the heteronuclear correlation. Even at such a short contact time, the modest amount of polarization transfer from CA to HN, HB, and HG is still evident in the slice shown in Figure 3a,b. In NAV, because of the especially long $T_1\rho$ relaxation on the ¹H reservoir (more than 10 ms), longer contact times could be used for the initial HC CP in the CH experiment to maximize the overall sensitivity. Nonetheless, a fractional transfer efficiency[16,19] of only $f_0 = 75\%$ can be achieved by using 2 ms contact time, which is comparable to values typically used in protein experiments (with ¹³C detection). In cases where protein samples suffer from further decreases in ¹H $T_1\rho$, methods such as recoupled polarization transfer[48,49] may be utilized to reduce signal loss in indirectly detected experiments.

The HN–N peak of NAV has an SNR value of 189 and 735, respectively, for the HN (Figure 4a) and NH (Figure 4b) 2D experiments. The enhancement is $\xi = 4.2$ after correction for the total number of scans using the same logic as earlier. The heteronuclear correlation was established with 0.3-ms HN CP, permitting a small percentage of polarization to leak to carbon-

(48) Saalwachter, K.; Graf, R.; Spiess, H. W. *J. Magn. Reson.* **2001**, *148*, 398–418.
(49) Schnell, I.; Langer, B.; Sontjens, S. H. M.; van Genderen, M. H. P.; Sijbesma, R. P.; Spiess, H. W. *J. Magn. Reson.* **2001**, *150*, 57–70.
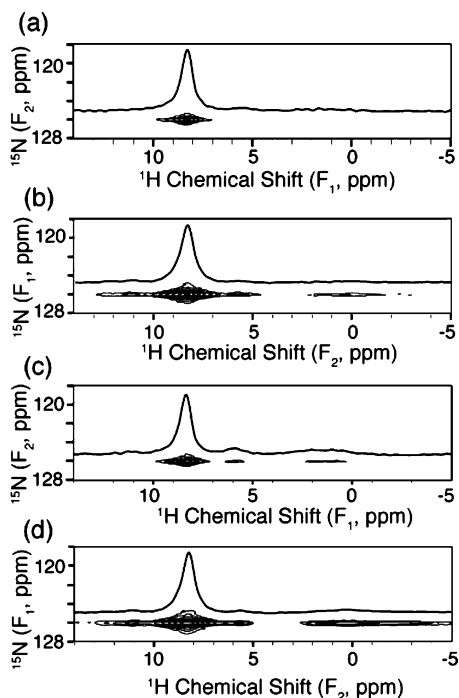
Figure 4. Heteronuclear $^{15}N-^{1}H$ 2D correlation spectra of fully protonated NAV (500 MHz ^{1}H frequency). Pulse sequences were used as reported previously,[34] with 40 kHz MAS, 2.2-s recycle delay, and 12.5-μs dwell time unless indicated otherwise. The indirect dimension was sampled with TPPI.[64] No apodization was applied in the processing. The lowest contour is drawn at 10σ and spaced by a factor of 2.0. (a) ^{15}N-detected HN 2D spectrum acquired with 324 t_1 increments, eight scans per row, and 0.3-ms HN CP contact time. (b) ^{1}H-detected NH 2D spectrum acquired with 548 t_1 increments, 200-μs dwell time, and four scans per row. The contact times were 1.6 ms for the initial HN CP and 0.3 ms for the final NH CP. (c) ^{15}N-detect HN 2D with 1-ms HN CP; other parameters were the same as those in (a). (d) ^{1}H-detected NH 2D with 1-ms NH CP; other parameters were the same as those in (b).

attached protons (mostly HA). This and other aliphatic proton signals do not compromise the HN resolution because of the differences in HN and HA chemical shifts. In proteins, transfer from amide nitrogen to interresidue amide protons is anticipated not to be problematic, for two reasons: first, the dipolar couplings from N[i] to HN[$i \pm 1$] are weaker than the N[i] to HA[i] couplings; second, the chemical shifts of the amide HN-[i] and HN[$i \pm 1$] protons are generally closer, thereby increasing the dipolar truncation effect (since the CP condition involving all the amide protons is encountered at the same rf field).[50] Therefore, even longer contact times could be used without increasing spectral overlap in the amide region. For example, data shown in Figure 4c,d were acquired with a contact time of 1 ms, resulting in SNR values of 1195 and 243 for ^{1}H and ^{15}N detection, respectively (where the ratio after correction of total number of scans is the sensitivity enhancement factor, $\xi = 5.3$).

B. Solvent Suppression Strategies. For hydrated solid protein samples, water suppression techniques have been developed with[51] or without[19] gradient pulses. The latter method utilizes an ~40-ms constant time t_1 period under ~100 kHz

TPPM[52] or XiX[53] decoupling for the saturation of water resonance.[19] In our hands, this sequence provides adequate suppression only for the water resonance, consistent with reports from Zilm and co-workers that deuterated MPD was required in studies of ubiquitin.[19] The effectiveness of this approach may depend upon rates of chemical and dipolar exchange between solvent and protein, which in general will vary with sample properties and temperature. To determine whether natural abundance precipitants could be utilized, we wished to modify the pulse sequences to suppress multiple solvent resonances simultaneously.

A second concern became apparent immediately upon attempting high-power ^{1}H decoupling at ~40 kHz MAS. Nutation frequencies of at least ~150 kHz were required to achieve satisfactory resolution with TPPM[52] or high-power XiX[53] conditions. Such decoupling levels, even with highly thermo-stable samples such as GB1 at a relatively modest 500 MHz frequency, caused excessive dielectric heating, as previously demonstrated for ubiquitin.[37] The first GB1 sample examined in this study was destroyed within minutes under these decou-pling conditions, although the same sample (previous to this decoupling test) and others in subsequent experiments yielded very high quality spectra (vide infra) over the course of many days of spinning at 40 kHz using lower power decoupling conditions. *Therefore, the high power decoupling, not the centrifugal forces or frictional heating associated with fast MAS, accounted for the sample damage.*

In the subsequent experiments, we utilized low-power XiX decoupling[42] at a nutation frequency of ~12 kHz, which was found to have a performance similar to that of high-power TPPM or XiX for all but the methylene carbon sites. With this decoupling strategy, 40 ms of 12 kHz rf irradiation was not sufficient to suppress solvent signals, and therefore we adapted a modified solvent suppression strategy (Figure 1) with the saturation pulses separated from the t_1 evolution time. During longitudinal storage of the X nucleus polarization, a long rf irradiation pulse (~300 ms) was applied at moderate nutation frequency (~40 kHz). Notably, this pulse also deposits a nontrivial amount of power into the sample, but at 40 kHz the power deposition per unit time is only ~7% of that at 150 kHz; therefore, 300 ms at 40 kHz is the equivalent of only 20 ms at 150 kHz decoupling on average, and avoids sudden bursts that may cause transient thermal damage over the time scale of 10−50 ms. The 40 kHz proton field is achieved with only 4 W incident power for the 1.6-mm probe (which has a 1.05 μs $\pi/2$ pulse at full power of 148 W); no change in the sample was found after three weeks under these conditions.

This modified solvent suppression scheme was found to suppress multiple solvent resonances satisfactorily, as demon-strated in Figure 5 by several proton spectra, showing the equivalent of the first row of 2D and 3D spectra acquired with the pulse sequences in Figure 1. In the one-pulse experiment (Figure 5a), solvent signals dominate the spectra, and the receiver dynamic range was not sufficient to detect the weaker protein signals. Figure 5b shows the ^{15}N-edited proton spectrum acquired with 40 ms of 100 kHz TPPM decoupling and an additional 10-ms T_2 filter according to the suppression method

(50) Hodgkinson, P.; Emsley, L. *J. Magn. Reson.* **1999**, *139*, 46−59.
(51) Chevelkov, V.; van Rossum, B. J.; Castellani, F.; Rehbein, K.; Diehl, A.; Hohwy, M.; Steuernagel, S.; Engelke, F.; Oschkinat, H.; Reif, B. *J. Am. Chem. Soc.* **2003**, *125*, 7788−7789.
(52) Bennett, A. E.; Rienstra, C. M.; Auger, M.; Lakshmi, K. V.; Griffin, R. G. *J. Chem. Phys.* **1995**, *103*, 6951−6958.
(53) Detken, A.; Hardy, E. H.; Ernst, M.; Meier, B. H. *Chem. Phys. Lett.* **2002**, *356*, 298−304.
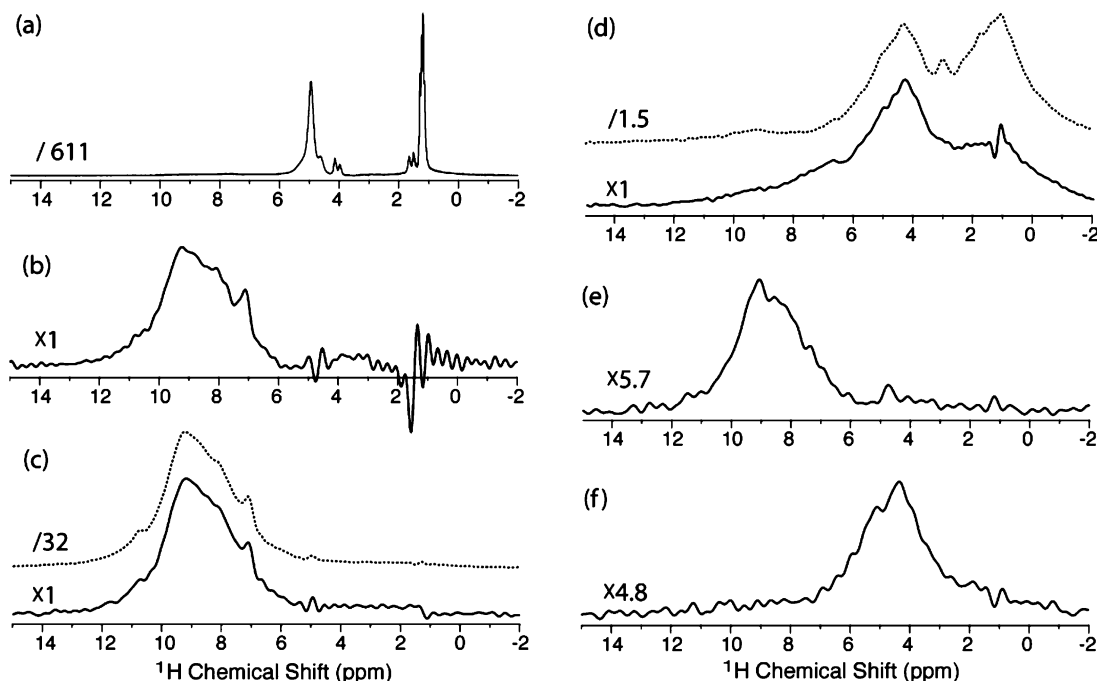
Figure 5. Proton 1D spectra of hydrated GB1 with and without solvent suppression. (a) Bloch decay spectrum without solvent suppression. (b) ^{15}N-edited ^{1}H spectrum using the published sequence,[19] which is equivalent to the scheme from Figure 1a without the first dephasing period τ_w. During the t_{1max} period, 100 kHz TPPM decoupling was applied.[52] The ^{1}H channel carrier frequency was placed at the water resonance, 0.3-ms NH CP. (c) ^{15}N-edited proton spectra using the pulse sequence of Figure 1a. Two and 64 scans were acquired for the solid and dotted spectra, respectively; 0.3-ms NH CP. (d) ^{13}C-edited ^{1}H spectra using the sequence of Figure 1a, 0.05- (solid) and 0.4-ms (dotted) CH CP. (e) CA- and ^{15}N-edited ^{1}H spectrum using the pulse sequence of Figure 1b, 0.3-ms NH CP. (f) [15]N- and CA-edited ^{1}H spectrum using the sequence of Figure 1b, 0.05-ms CH CP. Spectral scales in all cases are adjusted as indicated in the figure.

of Zilm and co-workers.[19] This represents a substantial improvement over the one-pulse experiment, but the remaining solvent intensities are comparable to the protein signals; in tests of 2D and 3D experiments with this scheme, we found substantial t_1 noise due to the variations in solvent suppression quality as a function of the evolution times. In contrast, ^{15}N-edited proton spectra were acquired in 2 and 64 scans (Figure 5c), respectively, using the sequence of Figure 1a, with low power XiX decoupling, a 300-ms saturation pulse at 40 kHz rf field, and an additional 10-ms T_2 filter. Only small residual solvent intensities remain at 4.9 and 1.3 ppm. The major contribution to the residual peak at ~4.9 ppm is signal transferred from protein to water, to be demonstrated further in the discussion of 2D NH spectra later in the article. Two ^{13}C-edited proton spectra (Figure 5d) were acquired with 0.05- and 0.4-ms CH CP, respectively, also using the pulse sequence of Figure 1a; similarly, high-quality solvent suppression was observed, and even HA signals near 5 ppm were detected with good dynamic range (and shown later in the article in correlation spectra detected on the ^{1}H spins). Doubly CA−N-edited and N−CA-edited proton spectra using the 3D pulse sequence in Figure 1b are shown in Figure 5e,f, respectively. Although it was not possible to remove the methyl proton signal intensity entirely, the small amount remaining at 1.3 ppm did not interfere with protein signals in the 2D and 3D spectra. Because of the quality of the solvent suppression pulse sequence, it was not necessary to apply solvent suppression in the data processing.

C. Resolution and Sensitivity in Protein Spectra. Indirectly detected NH and CH 2D spectra of the uniformly ^{13}C,[15]N-labeled protein GB1 (Figure 6) demonstrate substantial resolution despite the lack of deuteration. In Figure 6a, the majority of the N−H correlations are resolved by using a modest degree

of resolution enhancement in the processing (with details specified in the figure caption). The outlying peaks such as T49 and G14 are tentatively assigned on the basis of their solid-state ^{15}N chemical shifts[35] and confirmed through 3D experiments discussed later in the article. Confident peak assignments in the congested regions required 3D spectra. Likewise, some C−H correlations are well resolved in 2D experiments (Figure 6b), but the CA−HA region is generally congested because of the smaller chemical shift ranges of CA and HA than those of N and HN.

To compare sensitivity quantitatively, the HN and NH spectra were reprocessed with no apodization, using time-domain data sets digitized to a maximum evolution time of at least $3T_2$, based on the average T_2 values of 28 ms for the entire amide ^{15}N region and 0.68 ms for the HN region. Line widths (Δ) were measured from the well-resolved peaks as 18 ± 4 Hz (0.36 ± 0.08 ppm) for ^{15}N and 500 ± 150 Hz (1.0 ± 0.3 ppm) for [1]H (reporting mean $\pm$ standard deviation). The apparent relaxation time T_2^* was calculated from the average line widths (using $T_2^* = 1/(\pi\Delta)$) to be 17.3 and 0.64 ms for ^{15}N and HN, respectively; these values indicate that approximately 35% of the line width (~0.1 ppm) on the ^{15}N sites is due to inhomogeneous factors such as chemical shift dispersion or static magnetic field inhomogeneity (~0.05 ppm on this probe). The HN line widths are essentially all due to homogeneous relaxation, under these conditions still an order of magnitude greater than the inhomogeneous factors. The T_2^* values determined in this manner were then utilized to obtain the enhancement factor, by truncating the raw data to $3T_2^*$ and reprocessing. The SNRs were determined to be 217 ± 80 in the NH ([1]H-detected) spectrum and 68 ± 36 in the HN (^{15}N-detected) spectrum, based on the same set of resolved peaks.
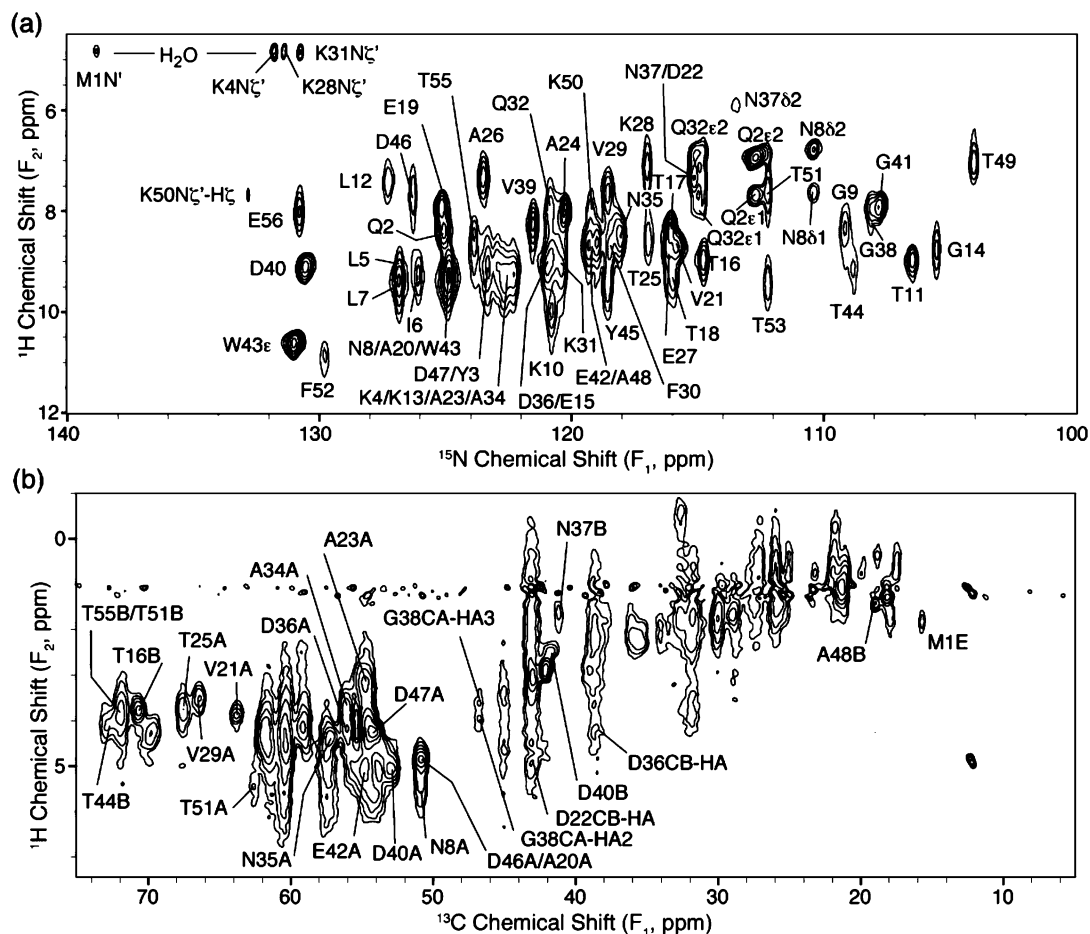
Figure 6. Heteronuclear 2D $^{15}N-^{1}H$ and $^{13}C-^{1}H$ correlation spectra for the nanocrystalline protein GB1 (5 mg, uniformly $^{1}H,^{13}C,^{15}N$-labeled) at 500 MHz ^{1}H frequency, 40 kHz MAS rate. The pulse sequence of Figure 1a was used, with a recycle delay of 1.5 s. The ^{1}H dimension was apodized by squared sine bell (shift = 45°) and Lorentzian-to-Gaussian transformation (-100 Hz Lorentzian, $+100$ Hz Gaussian). (a) ^{1}H-detected NH 2D spectrum acquired with 420 t_1 increments, 200-μs dwell time, 24 scans per row, 0.9-ms HN CP, and 0.3-ms NH CP. Contours are drawn starting at 20σ, with a spacing factor of 1.5. No apodization was applied to the ^{15}N dimension. Peaks labeled with a prime are fold from the upfield (amino) region. (b) ^{1}H-detected CH 2D spectrum acquired with 420 t_1 increments, 16 scans per increment, 12.5-μs dwell time, 0.9-ms HC CP, and 0.05-ms CH CP. Contours are drawn starting at 16σ with a spacing factor of 1.5. The ^{13}C dimension was apodized by sine bell (shift = 45°) and Lorentzian-to-Gaussian transformation (-25 Hz Lorentzian, $+25$ Hz Gaussian).

After correcting for the difference in total number of scans (6240 for NH and 9854 for HN), the enhancement factor was found to be $\xi = 4.2 \pm 0.8$. Performing the same comparison of HC (^{13}C-detected) and CH (^{1}H-detected) spectra, we found the proton detection sensitivity enhancement factor to be $\xi = 3.0 \pm 0.3$ as measured from nine resolved peaks. During the 300-ms saturation pulse, the longitudinal decay of ^{15}N or ^{13}C signals was slightly less than 10% (data not shown). This 10% loss can be recovered if other methods of solvent saturation (such as with gradients) could be used to avoid the long saturation period.

The amino region of the NH 2D spectrum (Figure 6a, peaks in the upper left region of the spectrum, labeled with a prime) was folded to the region downfield from the amides to expedite the acquisition. Peaks correlating the water resonance and amino ^{15}N were observed for lysine side chains (K31, K28, K4) and M1. It has been reported previously that protein–water magnetization transfer is dominated by the fast chemical exchange of labile protons.[22]

Longer NH CP contact times can be used to increase signal intensity without observing sequential or longer $^{1}H-^{15}N$ correlations (e.g., HN[$i \pm 1$] − N[i] or HN[j] − N[i], where |j −

i| > 1). In Figure 7, slices through the T49, G14, T11, G9, and F52 resonances were extracted from the NH 2D spectra acquired with two different CP contact times, 0.1 and 0.6 ms. The overlay of the data illustrates no changes to the line shapes within the random noise of the data (i.e., no new peaks are observed as the mixing time is increased from 0.1 to 0.6 ms). However, the sensitivity was increased by about 50%. Taking the average of 20 resolved peaks and normalizing the integrated peak intensity observed at 0.1 ms CP time, we found that the peak intensity increased to 1.3 ± 0.3 for 0.3 ms and 1.5 ± 0.3 for 0.6 ms. In many of the peaks, we noticed a foot at the base of the line shape, which could not be eliminated by ^{13}C or ^{15}N decoupling in the directly acquired dimension and varied from one site to the next, in a manner inconsistent with a static magnetic field (B_0) inhomogeneity, which can sometimes give rise to such observed line shapes for ^{13}C signals. However, neither the size of the effect nor the variations in the symmetry properties were consistent with the explanation of B_0 inhomogeneity. Rather, exact numerical simulations using SPINEVOLUTION[54] revealed that this line shape feature was caused by an oscillation of polarization among the neighboring amide protons assisted

(54) Veshtort, M.; Griffin, R. G. *J. Magn. Reson.* **2006**, *178*, 248−282.
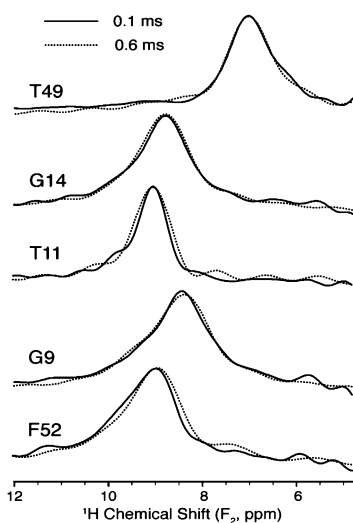
Figure 7. Proton 1D spectra taken from NH 2D acquired with 0.1-ms (solid) and 0.6-ms (dashed) NH CP. Other than CP time, experimental parameters were identical to those in Figure 6a. The 2D spectra were processed without any apodization.

by the local proton network. Details of this theoretical study will be reported elsewhere.

D. Proton Assignment Using 3D Spectra. Although sensitivity was greatly enhanced by ^{1}H detection, the 2D NH and CH experiments of fully protonated GB1 did not provide sufficient resolution or unique connectivity information to assign all ^{1}H resonances. To complete the assignments, we implemented a family of 3D experiments (CANH, CONH, and NCAH) in analogy to proton-detected pulse sequences commonly employed in solution NMR of proteins.[55] CANH correlates intraresidue CA, N, and HN (Figure 8a,b). CONH correlates interresidue C′[i − 1], N[i], and HN[i] as well as the side-chain carbonyl and amine groups for Asn and Gln residues (Figure 8c). NCAH correlates intraresidue N, CA, HA, and optionally side-chain protons when a long contact time is used (Figure 9). N and CA dimensions were sampled to a maximum evolution time of 1.5 T_2 (T_2 = 28 and 4.4 ms, respectively) and C′ to T_2 (29 ms). Two scans per row were acquired for NCAH with 1-ms final CP in Figure 9e. Two scans likely would have been sufficient for the other types of 3D spectra as well, although four scans per row were acquired for CANH with 0.3-ms CP in Figure 8a,b, CONH with 0.3-ms CP in Figure 8c, and NCAH with 0.05-ms CP in Figure 9a–c. The experiments performed with two scans per row were completed within 1 day each with adequate sensitivity owing to the factor of approximately three in signal enhancement offered by proton detection, despite the use of less than 1 μmol of sample.

The high resolution provided by ^{13}C and ^{15}N in either CANH or CONH helped to assign the majority of amide proton resonances unambiguously, including G41 and G38 in Figure 8a, E15 and D36 in Figure 8b, and G14-E15 and G9-K10 in Figure 8c. In some instances, two or more residues had overlapping CA and ^{15}N chemical shifts, such as K10 and Q32 in Figure 8b. Likewise, the N35−D36 and K31−Q32 peaks in Figure 8c have very similar C′ and ^{15}N chemical shifts. In these cases, the ^{1}H chemical shifts enhance resolution, and using the two 3D spectra together we found unambiguous assignments.

(55) Ikura, M.; Kay, L. E.; Bax, A. *Biochemistry* **1990**, *29*, 4659−4667.
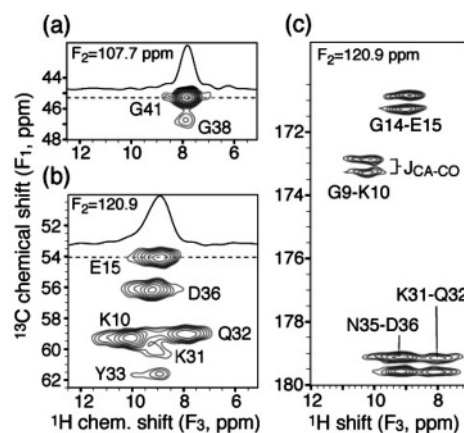
Figure 8. Representative 2D planes from 3D CANH and CONH spectra of GB1 (5 mg, uniformly ^{1}H,^{13}C,^{15}N-labeled), at 500 MHz ^{1}H frequency, 40 kHz MAS rate. (a) 2D plane (F_2 = 107.7 ppm) from 3D CANH spectrum with 1D slice through G41. Contours are drawn starting at 10σ with a factor of 1.3. (b) 2D plane (F_2 = 120.9 ppm) from 3D CANH spectrum with 1D slice through E15. Contours are drawn as those in (a). (c) 2D plane (F_2 = 120.9 ppm) from 3D CONH spectrum. Contours are drawn starting at 8σ with a factor of 1.2. The CANH spectrum (a and b) was acquired with 128 t_1 increments (50-μs dwell time) and 170 t_2 increments (250-μs dwell time), four scans per row, 0.3-ms NH CP. The CONH spectrum (c) was acquired with 96 t_1 increments (300-μs dwell time) and 170 t_2 increments (250-μs dwell time), four scans per row, 0.3-ms NH CP. For both experiments, the ^{1}H dimension was apodized by Lorentzian-to-Gaussian (−35 Hz Lorentzian, +75 Hz Gaussian) window functions. The indirect dimensions were forward linear predicted (eighth order, doubling the number of data points) and apodized by Lorentzian-to-Gaussian (−25 Lorentzian, +35 Hz Gaussian) window functions.

The CANH and CONH spectra are complementary because of the low likelihood of having identical chemical shifts for all C′[i − 1], CA[i], and HN[i]. For example, δ(HN) = 10.1 ppm could be unambiguously assigned to K10 from the CONH spectrum; Q32 was then assigned to 7.9 ppm in the CANH once the only other possibility (K10) was eliminated. In another case, the D36 amide was unambiguously assigned to 9.2 ppm in the CANH spectrum, enabling Q32 to be assigned in the CONH spectrum. Both approaches agreed in the assigned δ(HN) value for Q32, and similarly all amide protons could be assigned on the basis of these two 3D spectra. The proton assignments are listed in Table S1.

Each peak in the ^{13}C dimension of the CONH spectrum (Figure 8c) is a doublet due to the J-coupling between C′ and CA. In the experiments presented here, we did not attempt to perform scalar decoupling in the indirect ^{13}C dimensions of the 3D experiments, although the results clearly indicate that it would be possible to enhance both resolution and sensitivity further (by approximately a factor of 2) by implementing a selective π-pulse to decouple CA from C′.[56,57]

The NCAH spectrum acquired with short contact time (Figure 9a−c,e) was utilized to assign HA resonances. The plane at F_2(^{15}N) = 116.0 ppm (Figure 9a) resolves several CA−HA correlations such as T17, T18, V21, and E27. In addition, weaker CB−HB correlations for T17 and T18 appear in the downfield ^{13}C region. These HB signals appear despite the very short ^{13}C−^{1}H contact time because polarization was transferred from ^{15}N to CB during the SPECIFIC CP[41] period, as indicated by the CB chemical shifts. Notably, many of these HA resonances are

(56) Li, Y.; Wylie, B. J.; Rienstra, C. M. *J. Magn. Reson.* **2006**, *179*, 206−216.
(57) Zhou, D. H.; Kloepper, K. D.; Winter, K. A.; Rienstra, C. M. *J. Biomol. NMR* **2006**, *34*, 245−257.
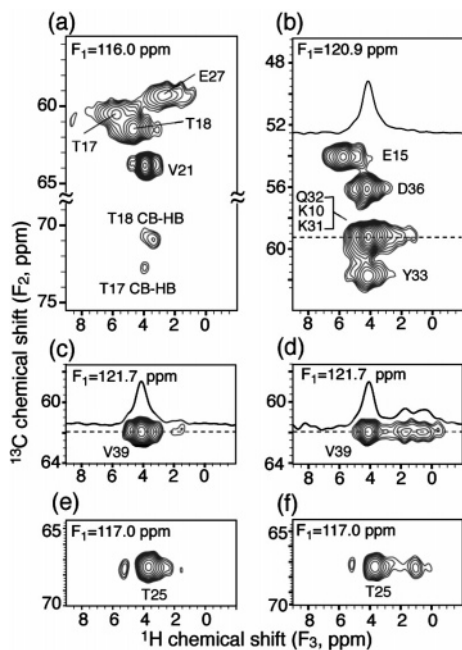
Figure 9. Representative 2D planes from 3D NCAH spectra of GB1 (5 mg, uniformly ^{1}H,^{13}C,^{15}N-labeled) at 500 MHz ^{1}H frequency, 40 kHz MAS rate. (a–c,e) Acquired with a 0.05-ms CH CP. (d, f) Acquired with 1.0-ms CH CP, enabling side-chain proton assignment. The pulse sequence of Figure 1b was used, where channel X is ^{13}C and Y is ^{15}N. Contours are drawn starting at 7σ with a spacing factor of 1.3. The spectra were acquired with 168 t_1 increments (250-μs dwell time) and 128 t_2 increments (50-μs dwell time), two scans per row. The ^{1}H dimension was apodized by Lorentzian-to-Gaussian (−35 Hz Lorentzian +75 Hz Gaussian) window functions. The indirect dimensions were forward linear predicted (eighth order, doubling the number of data points) and apodized by Lorentzian-to-Gaussian (−25 Lorentzian, +35 Hz Gaussian) window functions.

near the frequency of the water resonance, illustrating that excellent solvent suppression is key to identifying the HA and HB signals in the direct dimension. A second plane at $F_2(^{15}$N$)$ = 120.9 ppm (Figure 9b) illustrates correlations unambiguously assigned to E15, D36, and Y33; an additional set of three spin systems (Q32, K10, and K31) with similar ^{13}C and ^{15}N chemical shifts, as discussed earlier, is partially overlapped. Because of this overlap, the precision of chemical shift assignment in these cases is no better than 0.3 ppm, although the majority of sites could be determined to ±0.1 ppm precision.

Longer mixing time experiments were performed to identify side-chain protons, which are useful for probing dynamics and solvent interactions. At 1-ms CH CP contact time, transfer over several bonds was observed (notably, these distances from ^{13}C to ^{1}H are substantially less than the distances from ^{15}N to neighboring amide ^{1}H protons, as discussed earlier). The V39 and T25 spin systems illustrate these effects, by which the side-chain proton sites can be assigned. At the short (0.05 ms) contact time (Figure 9c) a very weak upfield (∼1.8 ppm) HB signal is observed in the V39 slice, and at the longer contact time (1 ms, Figure 9d) this signal increases to ∼50% of the intensity of the HA site. Furthermore, buildup of methyl HG intensity ranging from −0.5 to 1.0 ppm is observed. T25 resonances are shown in Figure 9e,f for 0.05 and 1-ms CH contact times, respectively. T25 has very similar chemical shifts for CA (67.2 ppm) and CB (67.8 ppm). Both N−CA−HA and N−CB−HB correlations are strong but overlapped in Figure 9e. Assignment of the HA and HB here relied upon knowledge of trends in the chemical shifts. An additional downfield peak (5.2 ppm) was
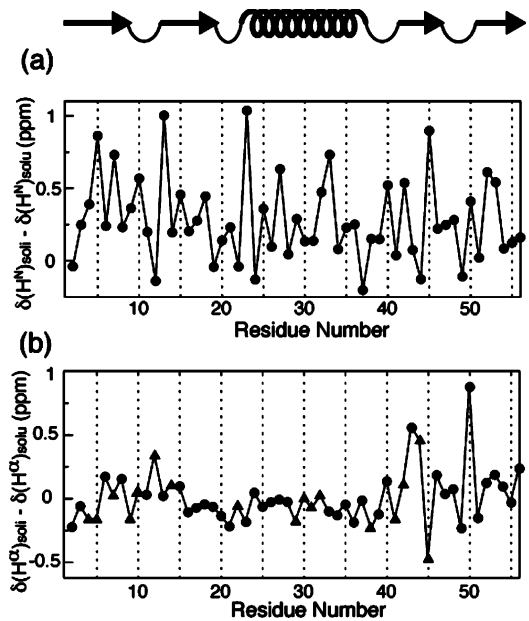
Figure 10. Backbone proton chemical shift difference between solid state and solution NMR for protein GB1. (a) Difference for amide protons. (b) Difference for HA; for glycines the average values of two α-protons were used. (●) Data points of small error (0.1 ppm). (▲) Data points of larger errors (0.3 ppm). A cartoon of the previously known secondary structure is also displayed.[38]

also observed at the short contact time and tentatively assigned to the hydroxyl HG1. The methyl HG2 intensity at 1.0 ppm was only observed at the longer contact time (Figure 9f). In all cases shown here, at the longer contact time, signals in the ^{1}H dimension cannot generally be unambiguously assigned because the polarization is transferred over at least 4 Å and therefore interresidue or long-range correlations may also be present. To resolve the long-range correlations uniquely would require greater resolution in the ^{1}H dimension and/or an additional ^{13}C or ^{15}N dimension, as in a previous study on α-spectrin SH$_3$ domain using ^{1}H−^{13}C−^{13}C 3D experiments.[58] Nevertheless, through combination of the 3D experiments we were able to assign all backbone ^{1}H signals (HN and HA) with a high level of confidence.

With the chemical shifts assigned in the solid state, the difference of $δ$(HN) and $δ$(HA) between solid and solution NMR were compared for each residue (Figure 10). All amide protons have been assigned unambiguously. The NCAH 3D spectrum was not sufficient to resolve all HA signals; as a result, 17 of the assignments were subject to larger uncertainty (±0.3 ppm) and represented by triangles in Figure 10b. Among the confidently assigned peaks (±0.1 ppm, circles in Figure 10b), W43 and K50 deviated significantly from solution chemical shifts. Chemical shifts were referenced to DSS for both states; for the solid-state data, the adamantane downfield ^{13}C peak was set to 40.48 ppm according to Morcombe and Zilm.[36] On average, the solid-state $δ$(HN) shifted *downfield* by approximately 0.2 ppm from solution state. This change could not be simply attributed to problems in chemical shift referencing, since it is not observed for $δ$(HA) in Figure 10b. It was previously reported that MPD tended in general to induce *upfield* changes in backbone amide ^{15}N and ^{1}H chemical shifts, which was

(58) van Rossum, B.-J.; Castellani, F.; Rehbein, K.; Pauli, J.; Oschkinat, H. *ChemBioChem* **2001**, *2*, 906−914.

Figure 11. Heteronuclear 2D ^{15}N–^{1}H correlation spectrum for the nanocrystalline protein GB1 (5 mg, uniformly ^{1}H,^{13}C,^{15}N-labeled) at 750 MHz ^{1}H frequency, 40 kHz MAS rate. The pulse sequence of Figure 1a was used, with 35 kHz saturation pulse applied for 250-ms, 2-s recycle delay. The ^{1}H dimension was apodized by squared sine bell (shift = 45°) and Lorentzian-to-Gaussian (50 Hz) window functions. Two scans were acquired for each of the 200 t_1 complex points with 25-μs dwell time; the direct dimension evolved to 4 ms, 0.7-ms HN CP, and 0.6-ms NH CP. A 45°-shifted sine bell was applied to the ^{15}N dimension. Contours are drawn starting at 30σ, with a spacing factor of 1.4.

attributed to changes in bulk solvent properties such as the dielectric constant.[59] Here we observe an opposite change in the solid state, for reasons that are not yet understood. The differences in δ(HN) between the two states are scattered, ranging from −0.25 to 1 ppm. It is consistent with the fact that δ(HN) is influenced by factors other than secondary structure, including electrostatics and solvent accessibility. The largest deviations are found for K13, A23, and Y45, which are in transitional regions of secondary structure and exposed to solvent and crystal contacts.

For the HA chemical shifts, a long stretch of residues from 16 to 39 shows relatively little deviation from solution state. This stretch consists of half of β2, the complete helix, and the two turns flanking the helix. There are very large deviations for residues from 43 to 50 that are in β3 and the loop connecting β3 and β4. This is in agreement with our previous observation of large CO, N, and CA chemical shift deviations in this region.[35] Overall, the differences in HN and HA chemical shifts from solution state observed here for GB1 have similar magnitude to those observed for SH3[60,61] with direct ^{15}N or ^{13}C detection.

E. Resolution and Sensitivity Benefits at High Magnetic Field. As a final experiment in this study, we performed indirect-detection experiments at 750 MHz proton frequency. The NH 2D spectrum (Figure 11) was acquired at 750 MHz on a replica of the sample used at 500 MHz, as the sample used for the 500 MHz experiments was damaged in the course of configuring the 750 MHz probe. Although we estimated that the quantity of protein (±5%) packed into this rotor was the same as that used on the 500 MHz instrument, more direct comparisons were not possible. The 750 MHz data was processed with modest resolution enhancement and compares favorably to the 500 MHz data in Figure 6a. Even when processed without any resolution enhancement, more than 36 peaks are resolved, double the number at 500 MHz. The line widths, extracted from the resolved peaks without apodization, are 360 ± 115 and 38 ± 6 Hz for ^{1}H and ^{15}N, respectively. The proton line widths are much narrower than the 500 ± 150 Hz observed at 500 MHz.

We attribute the difference in absolute line widths to truncation of homonuclear dipolar couplings by the larger chemical shift differences at the higher field. In relative terms, the line width decreased from 1.0 to 0.5 ppm. This additional relative narrowing is expected because the line widths are dominated by homogeneous factors (as judged by the ^{13}C spectra, which demonstrate ∼0.1 ppm inhomogeneous line widths, i.e., when acquired under optimal ^{1}H decoupling conditions). The absolute (Hz) and relative (ppm) effects on the ^{1}H line widths are each linear in magnetic field, and therefore the overall narrowing is quadratic with respect to the magnetic field strength. The ^{15}N line widths, however, broaden somewhat at 750 MHz data because of the greater challenge of properly decoupling the amide protons, as previously demonstrated by Zilm and co-workers.[19]

The sensitivity is 185 ± 77 as obtained from the data truncated to $3T_2$* in both dimensions, amounting to 416 total scans. This data was acquired with 0.6-ms contact time for the second CP. Therefore, a 500 MHz spectrum of 0.6-ms contact time was selected for comparison; the rest of the experimental parameters were identical to those in Figure 6a. Since ^{15}N line widths are broader for the 750 MHz data, to make a fair comparison with the 500 MHz data, we truncated and reprocessed the ^{15}N dimension of the 500 MHz data according to the 750 MHz T_2*. This resulted in a modified sensitivity for the 500 MHz of 285 ± 117 with 3096 total scans. Therefore, the ratio of sensitivity per scan is 185/285*(3096/416)$^{1/2}$ = 1.8. This factor of absolute sensitivity at the higher field can be attributed to the B_0^2 dependence (Boltzmann population on B_0 and electromotive force on Larmor frequency), yielding a factor of 2.25. A portion of this theoretical gain was lost because the 750 MHz probe was less efficient than the 500 MHz probe, generating 51% of the B_1 field at the same input power level; by the principle of reciprocity,[62] this leads to a significant loss in potential sensitivity. Conversely, it illustrates the potential for further gains upon optimization of resonators for high-frequency proton detection.

The overall enhancement factor at 750 MHz for ^{1}H versus ^{15}N detection was ξ = 14 ± 3, about 3.3 times greater than that at 500 MHz (ξ = 4.2 ± 0.8). This relative factor exaggerates the benefit of the higher magnetic field, because on the 750

(59) Xiao, T.; Gardner, K. H.; Sprang, S. R. *Proc. Natl. Acad. Sci. U.S.A.* **2002**, *99*, 11151−11156.
(60) van Rossum, B. J.; Castellani, F.; Pauli, J.; Rehbein, K.; Hollander, J.; de Groot, H. J. M.; Oschkinat, H. *J. Biomol. NMR* **2003**, *25*, 217−223.
(61) van Rossum, B. J.; Castellani, F.; Rehbein, K.; Pauli, J.; Oschkinat, H. *ChemBioChem* **2001**, *2*, 906−914.

(62) Hoult, D. I.; Richards, R. E. *J. Magn. Reson.* **1976**, *24*, 71−85.

MHz probe a scroll resonator was used, which has relatively low ^{15}N detection sensitivity. The ratio of ^{1}H to ^{15}N channel field per unit power was 0.50 at 750 MHz and 0.28 at 500 MHz. The narrower ^{1}H and broader ^{15}N line widths for the 750 MHz data also helped to increase ξ, since the value is proportional to $[\Delta(^{15}N)/\Delta(^1H)]^{1/2}$.[19] Together, the contributions of the relative probe efficiency and line widths are a factor of 3.1. Therefore, caution must be exercised when comparing the relative sensitivities as a function of magnetic field strength. Nevertheless, the important conclusion is that absolute sensitivity of the experiment increased by a factor of almost two upon increasing the magnetic field strength, using two nearly identical samples and equally well-optimized experiments.

Conclusions

The study presented here builds upon recently developed methods for detection of highly resolved proton signals in NMR spectra of solid peptides and proteins.[18,19,51] Here we performed experiments at 40 kHz MAS to investigate the feasibility of assigning amide and aliphatic proton signals without the requirement of deuterated samples. Model compound studies agreed well with expectations and identified optimal conditions for the protein studies, which demonstrated an enhancement in proton-detected experiments for GB1 to be 3.0 ± 0.3 versus ^{13}C and 4.2 ± 0.8 versus ^{15}N detection at 500 MHz. High-quality 2D ^{15}N$-^1$H correlation spectra at 500 MHz could be acquired in about an hour with less than 1 μmol of protein. Moreover, three 3D experiments were designed to establish systematic correlations among ^{13}C, ^{15}N, and ^{1}H (CANH, CONH, and NCAHA), enabling HA detection even of signals within 1 ppm of the solvent signals. Together, the 3D experiments enabled complete assignments of amide (HN) and HA resonances. The 3D experiments could be performed in under a day with high digital resolution in the indirect ^{13}C and ^{15}N dimensions, with no adverse effects to the sample from fast MAS.

Further improvements in sensitivity and resolution were observed in ^{15}N$-^1$H correlation spectra acquired at 40 kHz MAS rate and 750 MHz ^{1}H frequency, conditions enabling high-

quality 2D SSNMR protein spectra to be acquired in $\sim$30 min. The HN line widths in an absolute sense narrowed by $\sim$25%, from 500 ± 150 Hz at 500 MHz to 360 ± 115 Hz at 750 MHz. With this relative narrowing from 1.0 to $<$0.5 ppm, the majority of amide correlations in this 6.2 kDa protein could be uniquely resolved and identified. When normalized per unit measurement time to 1 h, the 750 MHz 2D ^{15}N$-^1$H spectra had an SNR of 260:1 and the 500 MHz spectra 150:1, representing a 73% increase in sensitivity per unit time at the higher frequency. These results bode well for studies of significantly larger proteins, as well as small proteins in relatively low concentrations. The 3D experiments (at 500 MHz) yielded $\sim$100:1 SNR values for GB1 in a day at 500 MHz. With the increase in performance at 750 MHz, a 50 kDa protein even with only half the sample density as GB1 would yield $\sim$10:1 SNR in the same experiment time. Combining the results shown here with previously established methods for measuring distance restraints among protons[63] offers the potential to solve solid-state protein structures without the requirement of deuteration at nonexchangeable sites.

Supporting Information Available: Example 2D planes from CANH, CONH, NCAH 3D spectra, and table of backbone proton chemical shift assignments for GB1 from both solid-state and solution NMR. This material is available free of charge via the Internet at http://pubs.acs.org.

JA073462M

(63) Lange, A.; Luca, S.; Baldus, M. *J. Am. Chem. Soc.* **2002**, *124*, 9704–9705.
(64) Marion, D.; Wuthrich, K. *Biochem. Biophys. Res. Commun.* **1983**, *113*, 967–974.
(65) Marion, D.; Ikura, M.; Tschudin, R.; Bax, A. *J. Magn. Reson.* **1989**, *85*, 393–399.
(66) States, D. J.; Haberkorn, R. A.; Ruben, D. J. *J. Magn. Reson.* **1982**, *48*, 286–292.